

A New Absolute Proper Motion Determination of Leo I Using HST/WFPC2 images and Gaia EDR3

DANA I. CASSETTI-DINESCU,^{1,2} CAITLIN K. HANSEN,¹ TERRENCE M. GIRARD,^{1,3} VERA KOZHURINA-PLATAIS,⁴
IMANTS PLATAIS,⁵ AND ELLIOTT P. HORCH¹

¹*Department of Physics, Southern Connecticut State University, 501 Crescent Street, New Haven, CT 06515*

²*Astronomical Institute of the Romanian Academy, Cutitul de Argint 5, Sector 4, Bucharest, Romania*

³*Department of Astronomy, Yale University, Steinbach Hall, P.O. Box 208101, New Haven, CT 06520-8101*

⁴*Space Telescope Science Institute, Baltimore, MD 21218*

⁵*Department of Physics and Astronomy, The Johns Hopkins University, Baltimore, MD 21218*

Submitted to AJ

ABSTRACT

We measure the absolute proper motion of Leo I using a WFPC2/HST data set that spans up to 10 years, to date the longest time baseline utilized for this satellite. The measurement relies on ~ 2300 Leo I stars located near the center of light of the galaxy; the correction to absolute proper motion is based on 174 *Gaia* EDR3 stars and 10 galaxies. Having generated highly-precise, relative proper motions for all *Gaia* EDR3 stars in our WFPC2 field of study, our correction to the absolute EDR3 system does **not** rely on these *Gaia* stars being Leo I members. This new determination also benefits from a recently improved astrometric calibration of WFPC2. The resulting proper-motion value, $(\mu_\alpha, \mu_\delta) = (-0.007 \pm 0.035, -0.119 \pm 0.026)$ mas yr⁻¹ is in agreement with recent, large-area, *Gaia* EDR3-based determinations. We discuss all the recent measurements of Leo I's proper motion and adopt a combined, multi-study average of $(\mu_\alpha^{3meas}, \mu_\delta^{3meas}) = (-0.036 \pm 0.016, -0.130 \pm 0.010)$ mas yr⁻¹. This value of absolute proper motion for Leo I indicates its orbital pole is well aligned with that of the Vast Polar Structure, defined by the majority of the brightest dwarf-spheroidal satellites of the Milky Way.

Keywords: Astrometry: space astrometry — Stellar kinematics: proper motions — Dwarf spheroidal galaxies: Leo I

1. INTRODUCTION

Highly precise and accurate proper-motion measures of distant Milky Way satellites remain difficult to come by in spite of the spectacular progress made by ESA's *Gaia* mission. The distances to these satellites places their stars at the faint end of the *Gaia* measurements where the proper-motion uncertainties are largest, making these systems challenging. Nevertheless, there are important science drivers for improving the state of proper-motion measurements for such systems as recently pointed out by Pawlowski & Kroupa (2020). One aspect highlighted by this study is the polar alignment of the most massive Milky Way (MW) satellites: the

more accurate the proper motions, the more apparent this alignment is. The co-orbiting of the most massive MW satellites is an observational aspect that challenges state-of-the-art cosmological simulations (Pawlowski & Kroupa 2020).

Although Pawlowski & Kroupa (2020) include *Gaia* DR2 proper motions (Gaia Collaboration et al. 2018a) in their work, two distant satellites stand out as having large uncertainties in the position of their orbit poles: Leo I and Leo II (see their Figure 1). Notably, Leo I's pole is outside the area where other satellites' poles cluster. Clearly, better measurements are needed for these two satellites.

In this study we will focus on Leo I. Our new proper-motion determination makes use of archival HST WFPC2 exposures spanning up to 10 years and *Gaia* EDR3 (Gaia Collaboration et al. 2021) to obtain the correction to absolute proper motion. A new distortion

calibration of WFPC2 (Casetti-Dinescu et al. 2021) is utilized. The WFPC2 exposures cover a small field of view very near the center of light of Leo I. This ensures that we only sample Leo I stars near the center of mass of the system. One advantage of this is to alleviate any offsets due to possible proper-motion gradients within Leo I’s internal kinematics over the field of study. Proper-motion studies of such satellites that rely directly on *Gaia* measurements of satellite stars are susceptible to such effects due to the trade off between the shallowness of *Gaia* and the areal coverage needed to obtain a reasonable number of member stars.

Radial velocity studies (Koch et al. 2007; Sohn et al. 2007; Mateo et al. 2008) do not find a significant spatial gradient in the line-of-sight velocity field for Leo I. Of course, this does not preclude the existence of a gradient in the tangential velocity field. Given the large areas over which candidate members are selected in *Gaia*-based proper-motion studies of dwarf galaxies, ($\sim r_{\text{tidal}}$ or more, see e.g., Martínez-García et al. 2021), we can estimate a rough upper limit as to the expected proper-motion gradient due to a plausible velocity gradient. To do so, we assume one of the largest gradients found in the Hercules system (Adén et al. 2009), specifically $16 \text{ km s}^{-1} \text{ kpc}^{-1}$. At the distance of Leo I, this corresponds to a delta of $0.012 \text{ mas yr}^{-1}$ for a spatial offset of r_{tidal} in the field of Leo I. This value approaches some of the proper-motion errors quoted for Leo I in the recent literature.

2. LITERATURE REVIEW OF LEO I PROPER-MOTION DETERMINATIONS

Previous measurements for Leo I are summarized in Table 1 and Figure 1. In Tab. 1 we present the reference, the data source, the proper motion values with formal uncertainties, the time baseline, the approximate number of Leo I stars and the approximate number of absolute proper-motion calibrators used in the determination. Calibrators can be *Gaia* stars or extragalactic sources. For completeness, we also include our study’s determination. Among the differences between the various *Gaia* DR2 or EDR3 studies are the ways in which Leo I members were selected: either spectroscopically, as for most studies, or via a combination of properties yielding a membership probability (McConnachie & Venn 2020b,a; Battaglia et al. 2021).

In Fig. 1 we present the 2013 HST determination by Sohn et al. (2013) compared to the *Gaia* DR2 (left panel) and *Gaia* EDR3 (right panel) determinations. The average value of the *Gaia* DR2 measurements is $(\mu_{\alpha}, \mu_{\delta}) = (-0.064 \pm 0.019, -0.122 \pm 0.021) \text{ mas yr}^{-1}$, where the uncertainties are from the standard deviation

of the four measurements¹. Specifically, the standard deviation is $(\sigma_{\mu_{\alpha}}, \sigma_{\mu_{\delta}}) = (0.037, 0.042) \text{ mas yr}^{-1}$, and can be interpreted as being due to the different ways in which Leo I members were selected. Otherwise, results should have been identical since they all use *Gaia* DR2 stars. Formal uncertainties for each *Gaia* DR2 determination are actually larger than the scatter indicates as they should also include any systematic errors in *Gaia* DR2. Since the average *Gaia* DR2 value is not obtained from independent measurements, it is best to assume its uncertainty is of the order of the standard deviation, or $\sim 0.04 \text{ mas yr}^{-1}$. In this case, the average *Gaia* DR2-based value is consistent with the 2013 HST measurement.

The *Gaia* EDR3-based determinations have smaller formal errors than the DR2 ones, with an average value $(\mu_{\alpha}, \mu_{\delta}) = (-0.054 \pm 0.006, -0.122 \pm 0.010) \text{ mas yr}^{-1}$, and a standard deviation $(\sigma_{\mu_{\alpha}}, \sigma_{\mu_{\delta}}) = (0.011, 0.020) \text{ mas yr}^{-1}$. The average value agrees very well with the *Gaia* DR2-based average, while the scatter is reduced by a factor of between two and four.

The one result somewhat discrepant from the other three is that of Martínez-García et al. (2021) who readjusts the absolute proper motion by using local (within a radius of 3 degrees) QSOs, rather than relying on the EDR3 direct measurements of Leo I stars. This is done in an attempt to eliminate any local systematic errors. Assuming once again an uncertainty in the *Gaia* EDR3 average value based on the standard deviation, the EDR3 value is found inconsistent with the 2013 HST measurement in μ_{α} at a 2σ level. A discrepancy of this size can alter the location of the orbital pole in a substantial way (see Section 7).

3. HST WFPC2 DATA SET

The WFPC2 served as the principal imaging instrument on the HST from 1993 to 2009, accumulating more than 135,000 exposures (see WFPC2 Data Handbook v10.0, MAST²). The WFPC2 consists of four different detectors, three of which are nearly identical. The three Wide Field Cameras at f/12.9 provide an “L” shaped field of view at $2.5' \times 2.5'$ with each $15 \mu\text{m}$ detector pixel subtending $0.10''$ on the sky. The Planetary Camera at f/28.3 provides a field of view of $35'' \times 35''$ with each pixel subtending $0.046''$ (see WFPC2 instrument handbook v10.0, Lindegren 2012).

¹ Throughout the paper μ_{α} actually represents $\mu_{\alpha} \cos \delta$, and units are mas yr^{-1} .

² Barbara Mikluski Archive for Space Telescopes, <https://archive.stsci.edu>.

Table 1. Leo I Proper-Motion Determinations

Reference	Data Sources	$\mu_\alpha \cos(\delta)$	μ_δ	Time Baseline	$N_{Leo\ I}$	N_{ZP}
Sohn et al. (2013)	ACS/WFC	-0.114 ± 0.029	-0.126 ± 0.029	5 years	~ 36000	~ 100
Gaia Collaboration et al. (2018b)	Gaia DR2	-0.097 ± 0.056	-0.091 ± 0.047	22 months	174	174
Fritz et al. (2018)	Gaia DR2	-0.086 ± 0.059	-0.128 ± 0.062	22 months	241	241
Simon (2018)	Gaia DR2	-0.013 ± 0.064	-0.091 ± 0.066	22 months	187	187
McConnachie & Venn (2020b)	Gaia DR2	-0.060 ± 0.070	-0.180 ± 0.080	22 months	15	15
McConnachie & Venn (2020a)	Gaia EDR3	-0.050 ± 0.010	-0.110 ± 0.010	34 months	15 ^a	15 ^a
Li et al. (2021)	Gaia EDR3	-0.066 ± 0.029	-0.107 ± 0.026	34 months	368	368
Martínez-García et al. (2021)	Gaia EDR3	-0.041 ± 0.030	-0.150 ± 0.024	34 months	294	594 ^b
Battaglia et al. (2021)	Gaia EDR3	-0.060 ± 0.010	-0.120 ± 0.010	34 months	1342	1342
this study	WFPC2 + EDR3	-0.007 ± 0.035	-0.119 ± 0.026	10 years	~ 2300	174+10 ^c

NOTE—All proper-motion determinations given in mas yr^{-1} . Column 1 lists the reference, Column 2 the source of the data, Column 3 and 4 give the proper motion in each coordinate with corresponding uncertainty estimates. In all but one of the Gaia determinations these estimates do not include potential systematic errors. Column 5 gives the time baseline, Column 6 gives the number of stars in Leo I considered members in the respective study (or the number of stars with membership probability $> 50\%$ for the [McConnachie & Venn \(2020b\)](#) and [Battaglia et al. \(2021\)](#) studies, Column 7 gives the number of objects (galaxies/QSOs/*Gaia* stars) used to derive the correction to absolute proper motion, i.e., zero point.

a - [McConnachie & Venn \(2020a\)](#) do not specify the number of Leo I members; we assumed the same number as in their previous 2020 study.

b - This study performs a local correction to absolute proper motion using QSOs within 3 degrees of Leo I's center, in an attempt to minimize potential systematic errors. Formal uncertainty estimates also include the effects of systematic errors.

c - Our study uses 174 *Gaia* stars and 10 galaxies.

The camera was deemed challenging for astrometry due to its undersampled CCDs ([Anderson & King 2000](#)) as well as due to large optical distortion ([Anderson & King 2003](#)) and charge transfer efficiency (CTE) effects ([Dolphin 2009](#)). Nevertheless, the WFPC2 archive offers a long time baseline for proper-motion studies, although this potential has yet to be fully exploited. Our team started a project to astrometrically recalibrate this instrument utilizing all suitable images in filters F555W, F606W, and F814W in combination with *Gaia* EDR3 ([Casetti-Dinescu et al. 2021](#)), thus enabling the possibility of new proper-motion studies using the WFPC2 archive (see below in 4). To this end, we searched the archive for a relevant science target represented by repeated exposures over a long time baseline, exposures that would include a reasonable number of *Gaia* stars. We decided to investigate the Leo I set of exposures, the properties of which are listed in Table 2. There are 12 F555W exposures separated by ~ 5 years and 16 F814W exposures separated by ~ 10 years.

In Figure 2 we show the field of view of our data set. Left and middle panels show the PC footprint of

Table 2. WFPC2 data set properties

PID	Filter	$N_{exp} \times T_{exp}(\text{sec})$	Epoch
5350	F555W	3×1900	1994.17
5350	“	1×350	“
8095	F555W	1×500	1999.46
8095	“	7×400	“
5350	F814W	3×1600	1994.17
5350	“	1×300	“
9817	F814W	4×600	2004.44
9817	“	4×500	“
9817	“	4×300	“

all F555W and F814W exposures respectively, with the PANSTARRS survey as background. The right panel shows the entire field of view as given by objects in our F555W proper-motion catalog. Leo I's center, adopted from [McConnachie & Venn \(2020b\)](#), is marked with a red cross in all panels. It is seen that all exposures have

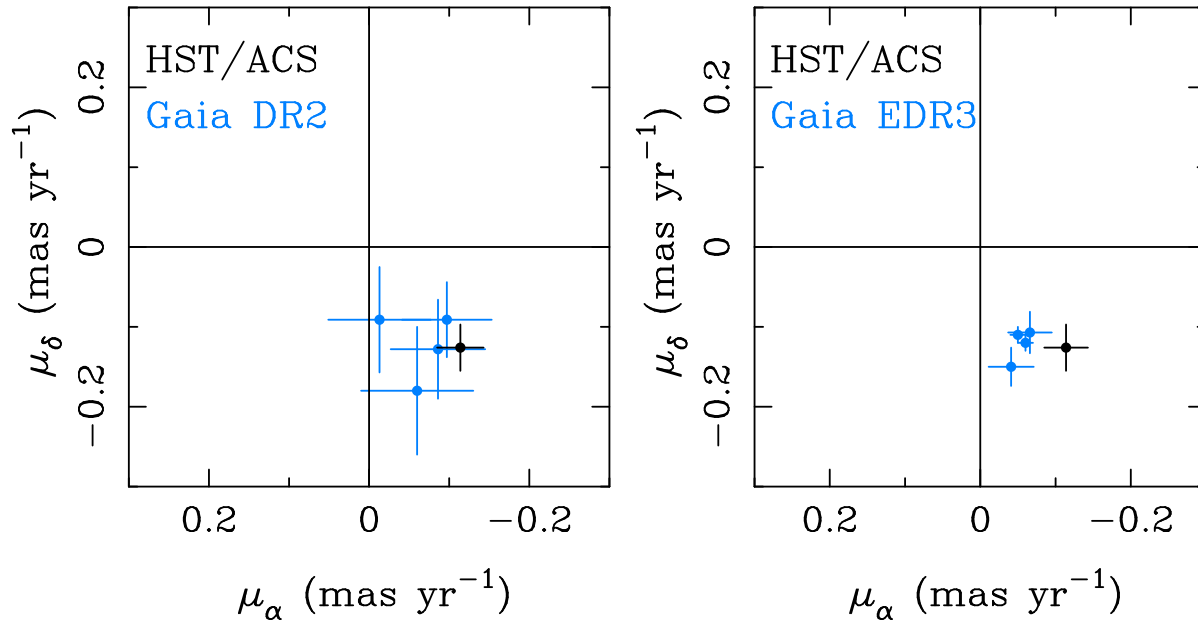


Figure 1. Absolute proper-motion determinations for Leo I. Besides the 2013 HST ACS/WFC determination, the left panel shows *Gaia* DR2-based measurements and the right panel shows those based on *Gaia* EDR3. Differences within the *Gaia* DR2 and EDR3 groups are primarily the manner in which Leo I members were selected. See also Table 1.

practically the same orientation and with very small offsets, of the order of a few arcseconds.

4. DATA PROCESSING

4.1. Detection and Centering of Stars in WFPC2 Exposures

The WFPC2 calibrated `_c0m.fits` images are downloaded from The Mikulski Archive for Space Telescopes (MAST) and split into separate chip files. Each WFPC2 chip is treated separately as an individual unit throughout our procedures. As stated in the WFPC2 instrument handbook, the pixels of the PC undersample the point spread function (PSF) by a factor of about two at visual wavelengths and the pixels of the WF chips undersample the PSF by a factor of about four at visual wavelengths. Therefore, we choose to employ the effective Point Spread Function (ePSF) code described by Anderson & King (2000) to determine a position and flux for each object in each exposure. This super-resolution code was developed specifically for undersampled images and has been shown to outperform other centering algorithms Casetti-Dinescu et al. (2021). The method uses an empirically-determined PSF that is fit to target images. For our purposes, the PSF used in the fitting process is based on a unique set of dithered HST/WFPC2 images combined into an ePSF library. Clearly, the ePSF library is best-suited for observations near the epoch of the data set used to construct it; this was early in the lifetime of WFPC2 on the HST. We note that this particular centering algorithm provides

very high precision centers for fainter stars, as seen empirically in the average residuals generated by transformations into standard catalogs (Casetti-Dinescu et al. 2021).

4.2. Astrometric corrections

There are a number of sources of systematic errors in the WFPC2 astrometry that are well-documented and modeled. The initial two adjustments to the WFPC2 positions are the 34th-row correction and the correction for nominal cubic distortion (Anderson & King 1999, 2003). The 34th-row correction accounts for a small manufacturing defect on each chip that made every 34th-row of pixels about 3% narrower. The nominal cubic distortion accounts for optically-induced geometric distortion of each of the WFPC2 chips. It is expressed as a filter-independent set of cubic coefficients, one set for each chip, that are listed in the WFPC2 instrument handbook. To further refine the WFPC2 positions, we then apply the recently determined geometric higher-order distortion-correction maps for each filter. These correction maps are based on *Gaia* EDR3 and all suitable WFPC2 exposures in the appropriate filter (Casetti-Dinescu et al. 2021).

Finally, we explore CTE effects in the WFPC2 positions. To do so, we adopt a first-epoch, long exposure as a reference exposure and transform all other exposures into it. The transformation is a classic polynomial one using as reference stars all well-measured stars on the CCD chip (see e.g., Casetti-Dinescu et al. 2018, and references therein). The vast majority of the stars in

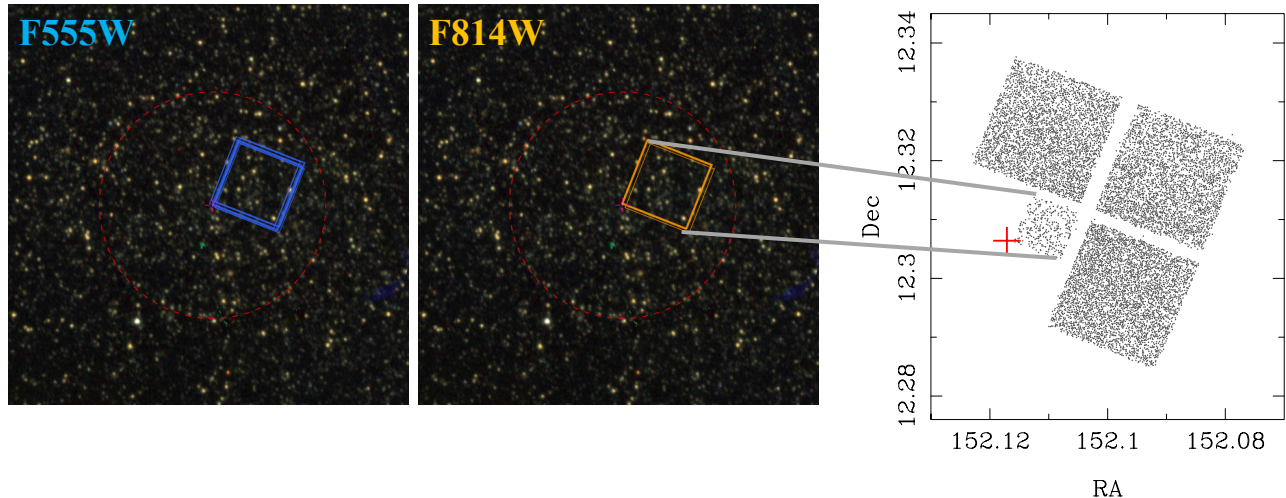


Figure 2. The field of view of our data set. The PC footprint of all F555W (left) and F814W (middle) exposures is highlighted with the PANSTARRS survey in the background. The right panel displays the entire field of view as represented by our resulting proper-motion catalog. The nominal center of Leo I is marked with a red cross in all panels. A circle of radius $60''$ is indicated in the left and middle panels for scale. For comparison, the half-light radius of Leo I is $198''$. All exposures have the same orientation, and offsets are of the order of a few arcseconds.

our exposures are Leo I members. The intrinsic proper-motion dispersion of Leo I stars is much lower than that given by position measurement errors. Therefore measurement error will dominate the scatter of the residuals of the transformation, even when epochs of the exposures differ. Trends of these residuals with magnitude should reveal systematics of the CTE type. When transforming an exposure near that of the reference exposure, the residuals are found to be flat in both chip coordinates; however, when comparing different epochs, slopes in residuals with magnitude are apparent in both x and y coordinates. We monitor these slopes for each chip and exposure and find that the slopes do vary from chip to chip, but do not change significantly from one late-epoch exposure to another. Thus we stack residuals per chip and filter, determining mean slopes and applying them as corrections to the positions of the late-epoch exposures. In Table 3 we present the values of these slopes. Note that the magnitudes are uncalibrated, instrumental magnitudes.

The physical interpretation of these values is not straightforward: y -slope values are not consistently larger than x -slope values as one would expect from CTE effects and the y direction being the readout direction (Recall that the orientation of all exposures is similar; see Sect. 3). Furthermore, the length of the exposure time did not make a difference in the values of the slopes. It appears that the epoch difference is the only factor that is relevant. The slopes are not very different between filters, although keep in mind the F814W set has twice as long a time baseline as the F555W set. Slopes also differ between individual WF chips. Possi-

Table 3. Slopes of late-epoch residuals as a function of magnitude.

Chip	x -slope (mpix/mag)	y -slope (mpix/mag)
F555W		
PC	-10.8 ± 1.7	-9.5 ± 1.4
WF2	2.9 ± 0.6	3.3 ± 0.6
WF3	8.6 ± 0.8	-4.8 ± 0.8
WF4	-2.9 ± 0.7	-7.1 ± 0.7
F814W		
PC	-7.5 ± 1.1	-9.8 ± 1.1
WF2	0.0 ± 0.5	3.6 ± 0.6
WF3	7.0 ± 0.7	-2.2 ± 0.8
WF4	-2.0 ± 0.6	-9.6 ± 0.7

bly, the ePSF changed substantially between early-90s and late-90s observations, and this is what the slopes reflect; although we cannot pinpoint what caused the ePSF change, be it CTE and/or some other effect. The slope corrections are empirically derived, from internal comparisons of the WFPC2 data.

Once positions are corrected for these magnitude-dependent linear trends, they all are on the system of the early-epoch exposures.

To check the impact of our magnitude-dependent correction we calculate relative proper motions (see also Sect. 5), rotate them into the celestial coordinate (RA,Dec) system using *Gaia* stars, and plot these as a

function of magnitude. If the corrections are appropriate, no trend with magnitude should be visible in the proper motions. In Figure 3 we show one such example, where the uncorrected proper motions are shown in the left panel, while the corrected ones are in the right panel. *Gaia* stars at the bright end are highlighted. After inspecting many such plots we conclude that the relative proper motions are largely free of any systematic trend. We note that the magnitude-slope corrections were derived (and applied) using residuals expressed in chip coordinates while the proper motions are in a rotated (RA, Dec) system. The degrees to which these proper-motion plots are flat with respect to magnitude is an indication that the correction was done adequately.

5. PROPER-MOTION DETERMINATION

5.1. *Relative Proper Motions*

The WFPC2 frames must be transformed to a common system in order to measure their proper motions differentially. We start by aligning the WFPC2 exposures in a detector-based coordinate system using a classical plate-overlap solution (e.g., Casetti-Dinescu et al. 2018, 2021). We utilize two early-epoch exposures, a 1900-sec exposure in F555W and a 1600-sec exposure in F814W, as our reference exposures. The assumption is that these exposures are least affected by CTE (e.g., Dolphin 2009).

The transformation consists of up to 3rd order polynomials. We estimate the plate constants³ by selecting reference stars on the detector field that are well-centered and with multiple measurements in our set of exposures. Stars with instrumental magnitudes ranging from 10 to 21 best fit these criteria. We use an iterative least squares procedure to refine the plate constants and the relative proper motions; in the initial iteration we assume zero proper motions for the reference stars.

Besides the WFPC2 exposures, we include in the procedure the *Gaia* EDR3 **positions**. The original *Gaia* EDR3 celestial coordinates (RA, Dec) are roughly transformed into detector coordinates (Casetti-Dinescu et al. 2021), and then treated as another “exposure” to the set of exposures for a given filter. In effect, the faint *Gaia* stars ($G = 18.4 - 21$) will benefit from having new relative proper motions derived from an increased baseline of ~ 20 years time difference, yielding very high precision proper motions, of the order of 0.1 mas yr^{-1} for the F814W set. This is an advantage that can be exploited in other, future relative proper-motion studies.

We determine proper motions for all objects with at least four position measurements separated by a 3 year minimum. We perform six iterations of the least-squares procedure with outlier culling at 2.5σ for the reference stars. Formal proper-motion uncertainties are calculated from the scatter about the best fit line in the position versus time plots. This process produces **relative** proper motion measurements in detector coordinates with units of millipixels per year. The output positions and proper motions are then converted to the celestial coordinate system (RA, Dec) via a transformation using the *Gaia* stars on each chip

The stars that participated in the plate solution are predominantly Leo I stars for the following reasons: the field is very near the center of mass of Leo I (see Fig. 2), the Galactic latitude of this field is rather high at 49° , the magnitude range is dominated by faint stars ($G > 18$), thus excluding foreground Galactic stars, and finally, the proper motion dispersion is very low (see Fig. 3) indicating a kinematically cold population, unlike the foreground Galactic stars. Therefore, our system of relative proper motions is roughly tied to the system of the Leo I dwarf spheroidal galaxy itself. In Figure 4 we show the relative proper motions for well-measured stars, highlighting the *Gaia* stars.

Next, we identify the Leo I stars that will be used in the determination of the average relative motion of the system. The selection of Leo I stars to include in this average is straightforward given that the target field is likely dominated by Leo I stars as we argued above. We calculate a simple average of the relative proper motions for each chip and filter. Outliers are removed based on the following criteria: instrumental magnitude > 21 in both filters, total proper motion error calculated as the square root of the squared values in each coordinate larger than 0.4 mas yr^{-1} and 0.8 mas yr^{-1} in the PC and WF respectively for filter F555W, and larger than 0.25 mas yr^{-1} and 0.5 mas yr^{-1} in the PC and WF respectively for filter F814W. After these cuts, we also remove stars with proper motions larger than 3σ from the average in an iterative fashion. Corresponding uncertainties in these averages are determined from the standard deviations of the measured proper motions. The average relative proper motion as determined per chip and per filter is presented in Table 4, where we have specified the number of stars used in each determination. Due to the smaller field of view of the PC compared to that of the WF chips, fewer stars are used in the PC solutions. The values in Tab. 4 are not far from zero, as expected, since the relative proper-motion solution used a frame of reference largely composed of Leo I stars. Still, the

³ These parameters are labeled as “plate” parameters to align with the historical use of the terminology when astrometry measurements were made with photographic plates.

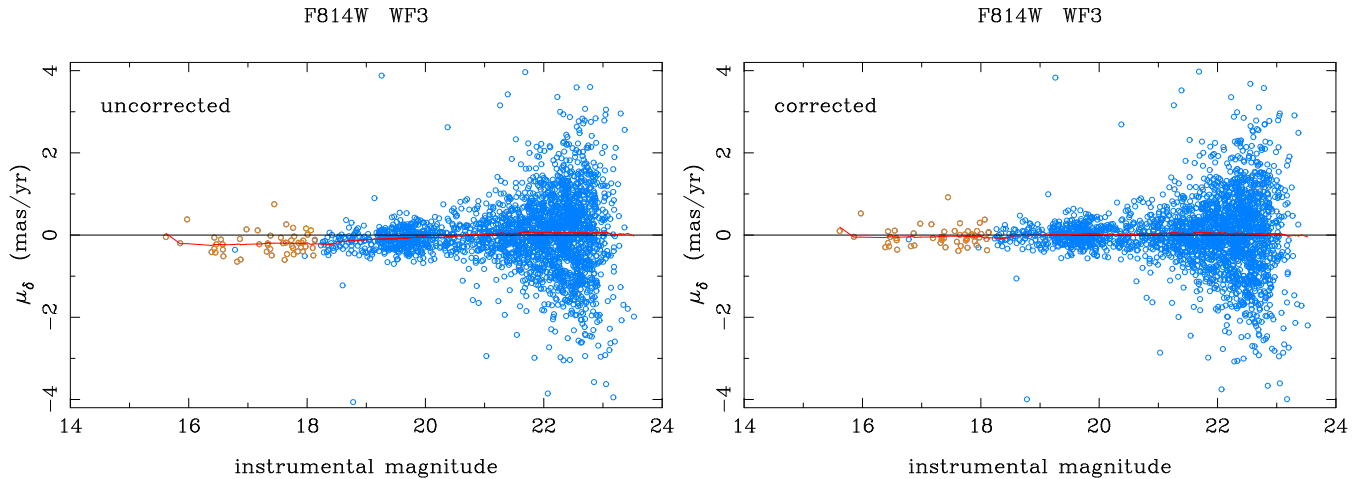


Figure 3. Relative proper motions, μ_δ , as a function of magnitude for filter F814W, chip WF3. **Left** panel shows the **uncorrected** values, **right** panel, those derived after **correcting** the late-epoch positions for the linear magnitude dependence. *Gaia* stars are highlighted with orange symbols. The red curve shows the magnitude trend via a moving mean. Similar plots were constructed and inspected for all chips, in component μ_α as well, and in filter F555W. Each exhibited roughly similar behavior. The *G*-magnitude range of the *Gaia* stars shown here is between 18.4 and 21.

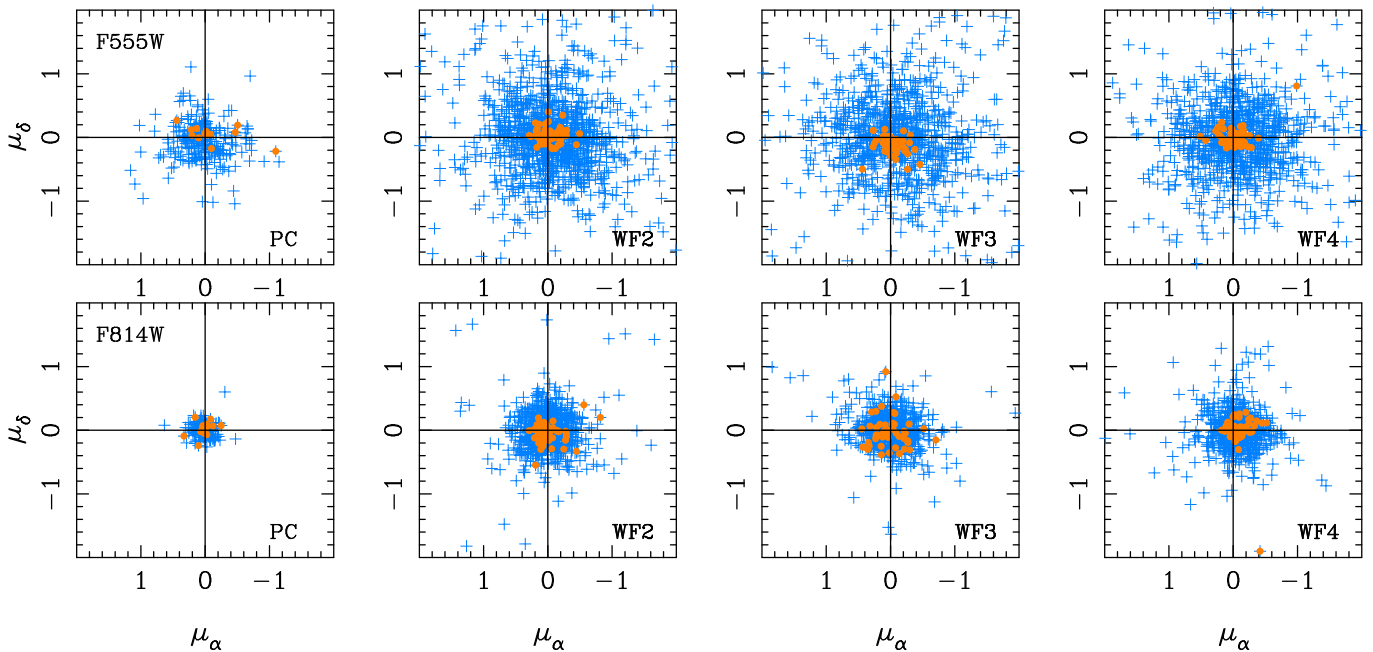


Figure 4. Relative proper-motion diagrams per chip and filter for objects with instrumental magnitude < 21 . *Gaia* stars are highlighted with round orange symbols. Units are mas yr^{-1} . F814W proper motions of non-*Gaia* stars are much tighter than those of F555W due to their having a 10-yr baseline compared to the 5-yr baseline for F555W.

calculation of a precise, relative proper-motion value for a properly cleaned sample of Leo I stars is important.

5.2. *Gaia*-based Absolute Proper Motion

To determine the proper motions with respect to an inertial reference frame, i.e., absolute proper motions, we make use of *Gaia* EDR3 stars. We calculate differences between the *Gaia* EDR3 absolute proper motions and our relative proper motions for *Gaia* stars that fall

on each chip, in each filter. The weighted average of these differences is used to determine the proper-motion offset, μ_{offset} , with separate offsets derived for each chip and filter. During the procedure, we eliminate outliers via an iterative 3σ clipping about a simple average, and then perform the weighted average. The weights are based on the square of the quadrature sum of the *Gaia* EDR3 catalog proper-motion uncertainties and the formal uncertainties of our relative proper motions. The

Table 4. Relative Proper-Motion Values of Leo I per chip and filter

Chip	F555W			F814W		
	$\mu_{\alpha,relative}$	$\mu_{\delta,relative}$	# of Stars	$\mu_{\alpha,relative}$	$\mu_{\delta,relative}$	# of Stars
PC1	0.040 ± 0.021	-0.026 ± 0.018	192	0.013 ± 0.009	-0.001 ± 0.008	149
WF2	-0.036 ± 0.016	0.001 ± 0.015	853	0.009 ± 0.009	-0.015 ± 0.009	724
WF3	-0.066 ± 0.021	-0.007 ± 0.019	586	-0.005 ± 0.011	-0.013 ± 0.009	568
WF4	-0.058 ± 0.018	-0.035 ± 0.016	684	-0.065 ± 0.010	-0.006 ± 0.009	592

Gaia errors dominate, with average values of the order of 0.75 mas yr^{-1} in RA and 0.53 mas yr^{-1} in Dec. Comparatively, our relative proper motion uncertainties are on average 0.1 mas yr^{-1} in both coordinates. We have also inspected the Renormalised Unit Weight Error (RUWE) values of the *Gaia* EDR3 stars. We remind the reader that RUWE values are expected to be around 1.0 for sources where the single-star model provides a good fit to the astrometric observations, while values > 1.4 indicate problematic sources for the astrometric solution [Lindegren et al. \(2021\)](#). We find that the RUWE values of our sample peak at 1.02, and of the 174 stars, only four have values larger than 1.2. Otherwise, we did not explicitly rely on the RUWE values in this process.

It is important to note that the *Gaia* stars participating in the determination of these offsets *need not be* Leo I stars, although probably the vast majority are, given the characteristics of this data set. The derived offset values are listed in Table 5. The PC offset values have the largest uncertainties due to the small number of *Gaia* stars and the fact that *Gaia* proper-motion uncertainties dominate the error budget.

We apply the offsets from Tab. 5 to the average relative proper-motion values listed in Tab. 4 to obtain an absolute proper motion for Leo I in each chip and filter. Uncertainties are given by the quadrature sum of the uncertainties in Tables 4 and 5. We list the resulting absolute proper-motion estimates in Table 6. For each filter, we also calculate a weighted average absolute proper motion across the four chips, where the weights are based on the uncertainties of each chip’s determination; results are listed in the last line of Tab. 6. In Figure 5 we show these various determinations. The PC estimates stand apart from the ensemble of the WF estimates, along with their larger uncertainties, nonetheless we choose to include them in the per-filter weighted average, realizing they contribute only slightly due to the weighting scheme. The weighted-average values for the two filters agree well, given their uncertainties.

5.3. Galaxy-based Absolute Proper Motion

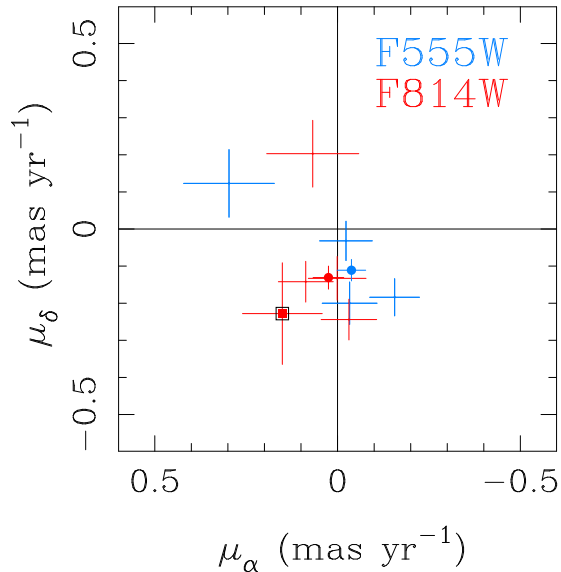


Figure 5. Absolute proper-motion determinations of Leo I. Our *Gaia* EDR3-based measurements are shown with 1σ error bars, color coded by filter. Each symbol represents a WFPC2 chip, the PC values lying in the upper left quadrant of the plot. The error-weighted averages, per filter, are represented by the large filled-circle symbols with smaller uncertainties. The square symbol shows the galaxy-based determination, which was made only with F814W images.

Background galaxies can also be used to determine the correction to absolute proper motion. Our WFPC2 data set is not well-suited for identifying compact galaxy images due to the severe undersampling. Nevertheless — using only the PC images — we median average the three deepest exposures from the first epoch in each filter and inspect them visually. We find four galaxies of which only one made it into our relative proper-motion catalogs. Alternatively, we make use of the galaxy classification from [Sohn et al. \(2013\)](#) who have kindly provided the necessary information for cross-matching. The [Sohn et al. \(2013\)](#) study is much deeper than ours, and also their ACS/WFC images are better sampled. We match our catalogs with that of [Sohn et al. \(2013\)](#) and, from their ~ 100 galaxies, we find 10 galaxies in common with our F555W list and 11 galaxies with our F814W

Table 5. *Gaia*-based proper-motion offset values, i.e., corrections to the absolute system

Chip	F555W			F814W		
	$\mu_{\alpha,offset}$	$\mu_{\delta,offset}$	# of Stars	$\mu_{\alpha,offset}$	$\mu_{\delta,offset}$	# of Stars
PC1	0.257 ± 0.122	0.149 ± 0.089	15	0.055 ± 0.126	0.204 ± 0.090	15
WF2	0.003 ± 0.073	-0.201 ± 0.055	52	-0.008 ± 0.078	-0.118 ± 0.058	51
WF3	0.043 ± 0.069	-0.025 ± 0.049	49	0.092 ± 0.074	-0.129 ± 0.054	47
WF4	-0.098 ± 0.066	-0.149 ± 0.047	57	0.034 ± 0.075	-0.238 ± 0.054	54

Table 6. *Gaia*-based absolute proper motion determinations per chip and filter

Chip	F555W		F814W	
	μ_{α}	μ_{δ}	μ_{α}	μ_{δ}
PC1	0.297 ± 0.124	0.123 ± 0.091	0.068 ± 0.126	0.203 ± 0.090
WF2	-0.033 ± 0.075	-0.200 ± 0.057	0.001 ± 0.079	-0.133 ± 0.059
WF3	-0.023 ± 0.072	-0.032 ± 0.053	0.087 ± 0.075	-0.142 ± 0.055
WF4	-0.156 ± 0.068	-0.184 ± 0.050	-0.031 ± 0.076	-0.244 ± 0.055
w.a.	-0.038 ± 0.039	-0.111 ± 0.029	0.025 ± 0.042	-0.131 ± 0.031

list. The small number of matches is due to the shallowness of our data set and the incomplete ($\sim 70\%$) areal overlap between the two studies. Specifically, our study has a Vegamag F814W magnitude range of 19.8 to 25.6, using the magnitude scale from [Sohn et al. \(2013\)](#). The single galaxy found on the PC in common with the [Sohn et al. \(2013\)](#) study is also the one we identified by visual inspection.

Since there are so few galaxies overall, we do not attempt per-chip estimates as in Sec. 5.2. Instead, we subtract from the entire set of relative proper motions the Leo I averages from Tab. 4, per chip, placing them all on a common system. Afterward, the ensemble of galaxies’ proper motions will, in effect, indicate the reflex proper motion of the Leo I system. Unfortunately, the galaxies’ F555W-based relative proper-motion errors are too large to allow a reliable zero-point determination; recall the shorter time baseline in this filter. For the F814W data, however, we are able to determine a useful, error-weighted average proper motion for the galaxies, after eliminating one obvious outlier. The resulting value is $(\mu_{\alpha}, \mu_{\delta}) = (0.151 \pm 0.109, -0.228 \pm 0.137)$ mas yr $^{-1}$, and represents Leo I’s absolute proper motion with respect to ten galaxies measured with the F814W set. Although the uncertainties are large, this measurement is consistent with the other per-chip and per-filter determinations and serves as a useful check on the *Gaia*-based

measurements. Our galaxy-based determination is also included in Fig. 5.

6. FINAL RESULTS AND COMPARISON WITH OTHER STUDIES

To produce a final estimate of Leo I’s absolute proper motion we must appropriately combine the *Gaia*-based results from Section 5.2, one in each filter, and the single galaxy-based estimate of Section 5.3.

Note that the *Gaia*-based estimates per filter are not independent since their uncertainties are dominated by the *Gaia* EDR3 catalog uncertainties, while the vast majority of *Gaia* reference stars are the same in the reductions of the two filter data sets. Specifically, there were seven *Gaia* stars that were in the F555W estimate and **not** in the F814W estimate, and there was one *Gaia* star that was in the F814W estimate and **not** in the F555W estimate. Thus, one cannot simply do an error-weighted average of the two filter’s values and naively propagate the errors to determine the error of the average.

To circumvent this difficulty we proceed as follows. We place all relative proper motions of the *Gaia* stars on a common proper-motion system, that of Leo I, by subtracting the values in Tab. 4 from their initial relative proper-motion values, in the same manner as in Sec. 5.3. At this point, all the stars’ proper motions will be on the same system, regardless of chip or filter. For each *Gaia* EDR3 star, we then do a weighted av-

erage of these “Leo I-system” proper motions for filter F555W and F814W, and propagate through the uncertainties. The weights are based on the relative proper-motion uncertainties in each filter. If the star only appears in one filter’s set, we simply retain that value. Next, for each *Gaia* star, we take the difference between its “Leo I-system” proper motion and its EDR3 catalog proper motion: this will be an estimate of the absolute proper motion of Leo I based on this single *Gaia* star. Its uncertainty is the quadrature sum of the relative (“Leo I-system”) and absolute (EDR3) uncertainties. There are a total of 174 such *Gaia* EDR3 stars for which proper-motion differences can be determined. We calculate an error-weighted average of these to produce a single, combined-filter, *Gaia*-based absolute proper motion of Leo I: $(\mu_\alpha^{EDR3}, \mu_\delta^{EDR3}) = (-0.025 \pm 0.037, -0.115 \pm 0.027)$ mas yr⁻¹.

As one would expect, this data point agrees well with the per-filter estimates (see Tab. 6 and Fig. 5), while the uncertainties properly take into account the substantial overlap in *Gaia* stars between the two filters’ samples. However, it must be noted that the *Gaia* EDR3 proper-motion system itself may have an unknown systematic error, i.e., offset from the inertial frame, at the location of Leo I. One way to get a handle on the expected size of such an error is from a fit to the covariances within EDR3 as a function of angular separation, as for instance given by Eq. 1 of Li et al. (2021). This yields an estimate of 0.022 mas yr⁻¹ for our field size. We do not explicitly include this in our uncertainty budget and simply adopt the *Gaia* EDR3 system as inertial. The reason for this is that we are not certain of the behaviour of Eq. 1 of Li et al. (2021) over a field of view as small as ours and because we will include in our final result information from ten galaxies.

Finally, we combine our *Gaia* EDR3-based motion with that based on galaxies from Sec. 5.3, doing once again a weighted average. Our final, combined result is: $(\mu_\alpha, \mu_\delta) = (-0.007 \pm 0.035, -0.119 \pm 0.026)$ mas yr⁻¹. We display this final result in Figure 6 together with the various large-area, *Gaia* EDR3-only measurements, and the earlier HST/ACS galaxy-based result. We also list our final result in Table 1.

While all measurements agree in μ_δ within errors, the recent *Gaia* EDR3-based results — including ours — tend to have more positive values in μ_α compared to the earlier HST/ACS result.

The question arises as to how best to combine the various measurements of Leo I’s absolute proper motion, as given in Table 1 and shown in Figure 6, if one desires the most useful value for the purpose of an orbit analysis, for instance. The *Gaia* DR2-based determinations are

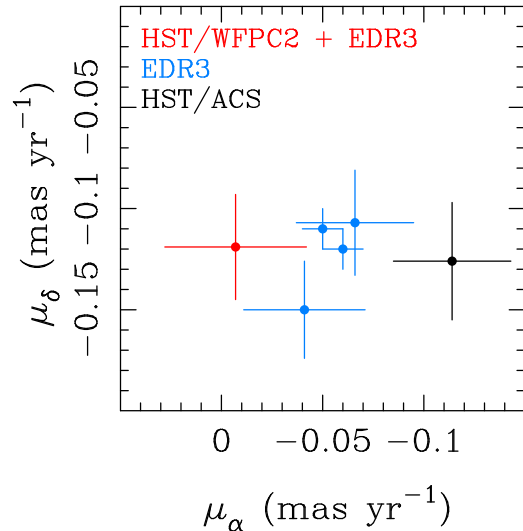


Figure 6. Absolute proper-motion measurements of Leo I: the galaxy-based HST/ACS 2013 one (black), the *Gaia* EDR3-only, large-area measurements (blue), and our current result (red). See also Tab. 1. Note the scale of the plot which is a zoomed-in version of Fig. 1.

clearly superseded by equivalent *Gaia* EDR3-based ones. Among the studies relying solely on *Gaia* EDR3 catalog proper motions of Leo I members, there is significant overlap and, hence, these are far from being independent measures. These studies, which differ primarily in the methods used to determine membership in Leo I over the large area associated with the satellite galaxy, include Battaglia et al. (2021); McConnachie & Venn (2020a) and Li et al. (2021). Among these three studies, only Li et al. (2021) takes into account systematic errors in *Gaia* EDR3 using a covariance function built from values in Lindegren et al. (2021). This is an internally-based estimation of systematic errors, and the outcome is that formal errors in the Li et al. (2021) study are 0.026 – 0.029 mas yr⁻¹, compared to those in the Battaglia et al. (2021) and McConnachie & Venn (2020a) studies which are 0.01 mas yr⁻¹ (see Table 1). Incidentally, the error estimates of Li et al. (2021) are in better agreement with the error estimates of Martínez-García et al. (2021) who include QSO’s to perform a local correction of the absolute proper motion system of *Gaia* EDR3.

Our recommendation is to choose one of these three (Battaglia et al. 2021; McConnachie & Venn 2020a; Li et al. 2021) measurements and combine it with the other, more independent measures, using a simple averaging and deriving the final uncertainty based on the scatter of the individual measures. This approach is justified by the near impossibility of disentangling any remaining dependencies between the various studies or to adequately judge the level of unaccounted for systematic effects that might be present. We select Battaglia et al.

(2021) as representative of the studies based on EDR3 catalog measures of assumed Leo I members, although either of the other two would have been equally valid. Next we include the determination by [Martínez-García et al. \(2021\)](#), in which a QSO-based correction to the local *Gaia* EDR3 zero point is made, giving this measure a significant degree of independence, and a means to keep systematic errors in check by incorporating external information given by the QSOs. Our own measure is included as it is focused on a tighter area near the center of Leo I, does not depend on *Gaia* EDR3 stars being members of the satellite, and is partially based on external galaxies as well.

Finally, there is the ACS/WFC determination by [Sohn et al. \(2013\)](#) to consider. As noted earlier in Sec. 2, its value of μ_α is rather discrepant relative to subsequent *Gaia* EDR3-based determinations. While it could be argued that it is only about 50% more discrepant than our own measure, we nonetheless choose to exclude it from the sample. This is partially motivated by the exercise of the following section in which the adopted absolute proper-motion is used to explore the pole of Leo I’s orbit. A previous study of Leo I’s orbit by [Pawlowski & Kroupa \(2020\)](#) effectively adopted the [Sohn et al. \(2013\)](#) proper-motion value by heavily weighting it. We wish to contrast this by examining the effect of adopting a proper-motion value that is predominantly *Gaia* EDR3-based and subsequently has a larger (positive) value of μ_α relative to the ACS/WFC determination. The following Section will demonstrate the sensitivity of the orbit pole analysis to using such an absolute proper-motion value.

The simple mean of the selected three measures of Leo I’s absolute proper motion, together with the formal error from the standard deviation about the mean, is: $(\mu_\alpha^{3meas}, \mu_\delta^{3meas}) = (-0.036 \pm 0.016, -0.130 \pm 0.010)$ mas yr⁻¹. The estimated uncertainties correctly reflect the larger overall scatter of the μ_α component compared to that of μ_δ .

7. ORBITAL POLE

A discussion of the orbit of Leo I is beyond the scope of this paper. We will address, however, one aspect of the orbit, namely the location of the orbital pole which is of importance when analyzing the ensemble of orbital poles of Milky-Way satellites. The clumpiness of the MW’s most massive satellites’ orbital poles is referred to as the Vast Polar Structure (VPOS), and indicates coherence in the motion of these satellites. [Pawlowski & Kroupa \(2020\)](#) determine the location of the 7 most-clumped satellite poles at Galactic coordinates $(l, b)_{VPOS}^{PK20} = (179.5^\circ, -9.0^\circ)$. This is for the “com-

Table 7. Orbit-Pole Input Parameters

Parameter	Value
l (degs)	225.986
b (degs)	49.112
D_\odot (kpc)	254 ± 16
V_{LOS} (km s ⁻¹)	282.5 ± 0.1

bined” sample, i.e., *Gaia* DR2 measurements and best available HST and other measurements (see their Table 3).

We calculate a new pole location for Leo I based on the proper motion values obtained in Sec. 6. The input parameters for Leo I are listed in Table 7, where the heliocentric distance and line of sight velocity are from [Pawlowski & Kroupa \(2020\)](#) and references therein. Likewise, in the calculation of the Galactic position (X, Y, Z) and velocity components (V_x, V_y, V_z) , we will use the same solar constants as in [Pawlowski & Kroupa \(2020\)](#), in order to have a meaningful comparison. These are: the local standard of rest (LSR) velocity $V_{LSR} = 239$ km s⁻¹, the solar peculiar motion with respect to the LSR $(V_{x,\odot}, V_{y,\odot}, V_{z,\odot}) = (11.10, 12.24, 7.25)$ km s⁻¹, and the location of the Sun from the Galactic center $d_\odot = 8.3$ kpc.

In Table 8 we present the orbital pole calculations for three different values of the absolute proper motion of Leo I: the value determined in this study (Sec. 6), the average of the selected *Gaia* EDR3 three most-independent measurements (Sec. 6), and the value used for Leo I in [Pawlowski & Kroupa \(2020\)](#). The latter value is dominated by the ([Sohn et al. 2013](#)) ACS/HST measurement as error-based weights were employed by [Pawlowski & Kroupa \(2020\)](#) in averaging the measurement of Leo I, and the ACS/HST measurement had the smallest ones.

Tab. 8 lists these proper-motion determinations and the Galactic rest frame velocity components with corresponding uncertainties in the first six columns. The next columns present the (l, b) of the pole, the separation angle (Δ) between this pole and the location of the average of the seven most-clumped satellite poles $(l, b)_{VPOS}^{PK20}$ from [Pawlowski & Kroupa \(2020\)](#). Finally, in the last column we list the standard deviation of the separation, which is determined in a Monte Carlo fashion by generating 1000 realizations drawn from a Gaussian distribution of the errors in proper motions, distance, and line-of-sight velocity. The scatter in the separation is dominated by the proper-motion errors. There is an

additional uncertainty of 16° in the adopted value of $(l, b)_V^{PK20}$ (Pawlowski & Kroupa 2020) to consider.

Leo I’s orbital pole as determined by Pawlowski & Kroupa (2020) from the combined *Gaia* DR2 (Gaia Collaboration et al. 2018a) and HST/ACS (Sohn et al. 2013) measurements is outside the clumped region of the orbital poles of the majority of the bright MW satellites (see also Fig. 1 in Pawlowski & Kroupa 2020). However, the new proper-motion determinations place Leo I’s orbital pole in much better agreement with the alignment of the other MW satellites (Tab. 8), further reinforcing the coherence of the VPOS structure. With the improved formal proper-motion uncertainties, the pole determination is also better constrained.

8. SUMMARY

We determine the absolute proper motion of Leo I using HST/WFPC2 exposures in F555W and F814W spanning up to 10 years. The astrometry benefits from a new calibration of the WFPC2 camera (Casetti-Dinescu et al. 2021). The absolute proper-motion zero point is based on 174 *Gaia* EDR3 stars and 10 galaxies. We also include between ~ 2000 and 2300 Leo I stars in this determination. Some of the advantages of our determination are:

- measuring a large number of Leo I stars with precise relative proper motions that allow us to cleanly separate Leo I members and field stars;
- focusing on a small area near the center of light of the galaxy, thus avoiding potential problems with proper-motion gradients and the need to correct for the center-of-mass motion;
- using an absolute proper-motion correction based on *Gaia* EDR3 stars, but one that does *not* require them to be Leo I members;
- providing also, as a check, a measurement based on ten background galaxies.

Our final result for the absolute proper-motion of Leo I is: $(\mu_\alpha, \mu_\delta) = (-0.007 \pm 0.035, -0.119 \pm 0.026)$ mas yr^{-1} . We combine this result with that of two other recent measurements from the literature to obtain a multi-study estimate of: $(\mu_\alpha^{3meas}, \mu_\delta^{3meas}) = (-0.036 \pm 0.016, -0.130 \pm 0.010)$ mas yr^{-1} . An orbital-pole analysis shows that either of these two proper-motion values indicates that Leo I exhibits motion coherent with the VPOS, thus reinforcing the significance of this structure.

ACKNOWLEDGMENTS

Support for program HST-AR-15632 was provided by NASA through a grant from the Space Telescope Science Institute, which is operated by the Association of Universities for Research in Astronomy, Inc.

This study has made use of data from the European Space Agency (ESA) mission *Gaia* (<https://www.cosmos.esa.int/gaia>), processed by the Gaia Data Processing and Analysis Consortium (DPAC, <https://www.cosmos.esa.int/web/gaia/dpac/consortium>). Funding for the DPAC has been provided by national institutions, in particular the institutions participating in the *Gaia* Multilateral Agreement.

We are very grateful to Tony Sohn for making available the list of galaxies from their 2013 study.

Facilities: HST (WFPC2), MAST, *Gaia*

Table 8. Velocities, Orbital Pole Location and Separation from $(l, b)_{VPOS}^{PK20}$

Solution	μ_α (mas yr ⁻¹)	μ_δ (mas yr ⁻¹)	V_x (km s ⁻¹)	V_y (km s ⁻¹)	V_z (km s ⁻¹)	l_p (°)	b_p (°)	Δ (°)	σ_Δ (°)
this study	-0.007 ± 0.035	-0.119 ± 0.026	-67 ± 32	-7 ± 32	173 ± 26	156	-19	24	13
ave. 3 meas.	-0.036 ± 0.016	-0.130 ± 0.010	-90 ± 14	-25 ± 14	148 ± 13	175	-31	22	9
PK20	-0.110 ± 0.026	-0.116 ± 0.025	-168 ± 27	-25 ± 27	102 ± 22	251	-39	70	14

REFERENCES

- Adén, D., Wilkinson, M. I., Read, J. I., et al. 2009, *ApJL*, 706, L150
- Anderson, J., & King, I. R. 1999, *PASP*, 111, 1095
- . 2000, *PASP*, 112, 1360
- . 2003, *PASP*, 115, 113
- Battaglia, G., Taibi, S., Thomas, G. F., & Fritz, T. K. 2021, arXiv e-prints, arXiv:2106.08819
- Casetti-Dinescu, D. I., Girard, T. M., Kozhurina-Platais, V., et al. 2021, *PASP*, 133, 064505
- Casetti-Dinescu, D. I., Girard, T. M., & Schriefer, M. 2018, *MNRAS*, 473, 4064
- Dolphin, A. E. 2009, *PASP*, 121, 655
- Fritz, T. K., Battaglia, G., Pawlowski, M. S., et al. 2018, *A&A*, 619, A103
- Gaia Collaboration, Brown, A. G. A., Vallenari, A., et al. 2018a, *A&A*, 616, A1
- Gaia Collaboration, Helmi, A., van Leeuwen, F., et al. 2018b, *A&A*, 616, A12
- Gaia Collaboration, Brown, A. G. A., Vallenari, A., et al. 2021, *A&A*, 650, C3
- Koch, A., Wilkinson, M. I., Kleyna, J. T., et al. 2007, *ApJ*, 657, 241
- Li, H., Hammer, F., Babusiaux, C., et al. 2021, *ApJ*, 916, 8
- Lindgren, L. 2012, *Astrometric satellites*, 14–28
- Lindgren, L., Klioner, S. A., Hernández, J., et al. 2021, *A&A*, 649, A2
- Martínez-García, A. M., del Pino, A., Aparicio, A., van der Marel, R. P., & Watkins, L. L. 2021, *MNRAS*, 505, 5884
- Mateo, M., Olszewski, E. W., & Walker, M. G. 2008, *ApJ*, 675, 201
- McConnachie, A. W., & Venn, K. A. 2020a, *AJ*, 160, 124
- . 2020b, *Research Notes of the American Astronomical Society*, 4, 229
- Pawlowski, M. S., & Kroupa, P. 2020, *MNRAS*, 491, 3042
- Simon, J. D. 2018, *ApJ*, 863, 89
- Sohn, S. T., Besla, G., van der Marel, R. P., et al. 2013, *ApJ*, 768, 139
- Sohn, S. T., Majewski, S. R., Muñoz, R. R., et al. 2007, *ApJ*, 663, 960